Large displacement model for the nonlinear behaviour of the face plate component

da Silva, Luís Simões; Tankova, Trayana

DOI
10.1016/j.jcsr.2024.108776

Publication date
2024

Document Version
Final published version

Published in
Journal of Constructional Steel Research

Journal of Constructional Steel Research 219 (2024) 108776

Contents lists available at ScienceDirect

Journal of Constructional Steel Research

journal homepage: www.elsevier.com/locate/jcsr

Large displacement model for the nonlinear behaviour of the face plate component

Luís Simões da Silva [a,*], Trayana Tankova [b]

[a] University of Coimbra, ISISE, Department of Civil Engineering, Portugal
[b] Delft University of Technology, Department of Engineering Structures, Netherlands

ARTICLE INFO

Keywords:
Component method
Connections
Face plate component
Minor axis joints
Tubular joints

ABSTRACT

This paper deals with the face plate component in steel joints and addresses the full characterization of the nonlinear behaviour of the face plate component. An equivalent beam strip model is proposed that tackles the connection of a beam to the column web of open I-sections in a minor axis joint or the face of tubular columns, covering endplate or fin plate joint typologies. Closed-form analytical solutions are obtained for the elastic large displacement and the elastic-plastic large displacement behaviour of the equivalent beam strip. Criteria for the establishment of the design resistance using the continuous strength method are also proposed. It was concluded that the model is easy to apply, was validated against a large parametric study using finite element beam models, leads to accurate solutions and demonstrates the need to consider membrane effects in design.

Notation

A_v	shear area, mm^2
B	axial force in bolt, kN
E	Young's modulus, MPa
F	transverse force from fin plate or horizontal plate, kN
F_{pl}	plastic resistance, kN
G	shear modulus, MPa
I	moment of inertia, mm^4
K_{ini}	initial stiffness, N/mm
K_m	membrane stiffness, N/mm
L_{eff}	length of equivalent strip, mm
b_p	width of face plate, mm
b_{hp}	width of horizontal plate, mm
c	length of area of patch load, mm
d	width of area of patch load, mm
d_m	equivalent diameter of bolt head, mm
e	width of beam, mm
f_y	yield strength, MPa
h_{hp}	depth of fin plate, mm
k	stiffness of the elastic foundation per unit length, N/mm^2
n	distance between the bolt axis and the edge of the face plate; distance between the edge of a horizontal plate and the edge of the face plate; distance between the axis of a fin plate and the edge of the face plate;
p	bolt pitch, mm
s	rotational stiffness per unit length of face plate longitudinal supports, kN/rad
t	Thickness of face plate, mm
t_{fp}	thickness of fin plate, mm
t_{hp}	thickness of horizontal plate, mm
α	ratio between the length of the area of the patch load and the width of face plate
β	ratio between the width of the area of the patch load and the width of face plate
θ	dispersion angle
μ	ratio between the width of face plate and the thickness of the face plate
ν	Poisson coefficient

1. Introduction

The behaviour of steel beam-to-column joints is often governed by the face plate component which is present whenever a steel member is connected to the web of an open I-section or to the face of a rectangular hollow section [1], as shown in Fig. 1. Yet, at present there is no guidance for the flexibility and resistance of this component in the European codes [2], even though several studies were presented in the past

* Corresponding author at: Civil Engineering Department, University of Coimbra, 3030-799 Coimbra, Portugal.
E-mail address: luisss@dec.uc.pt (L.S. da Silva).

https://doi.org/10.1016/j.jcsr.2024.108776
Received 14 February 2024; Received in revised form 25 April 2024; Accepted 15 May 2024
Available online 20 May 2024

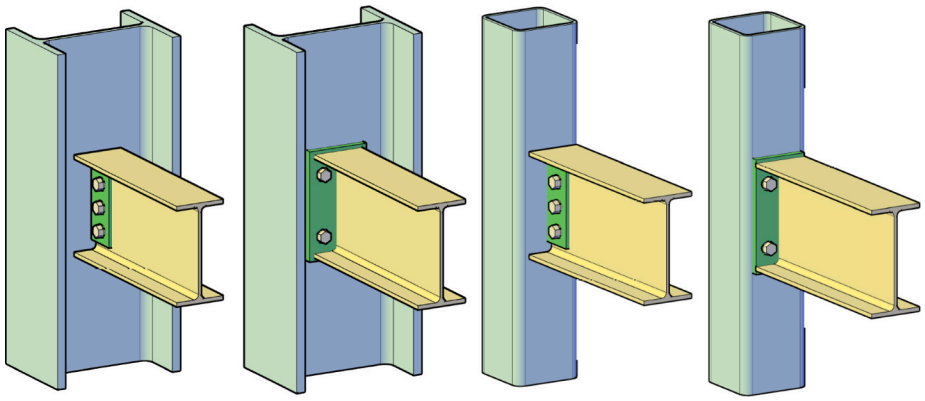

Fig. 1. Typical cases of connections to the web of an I section or the face of a tube (reproduced from [1]).

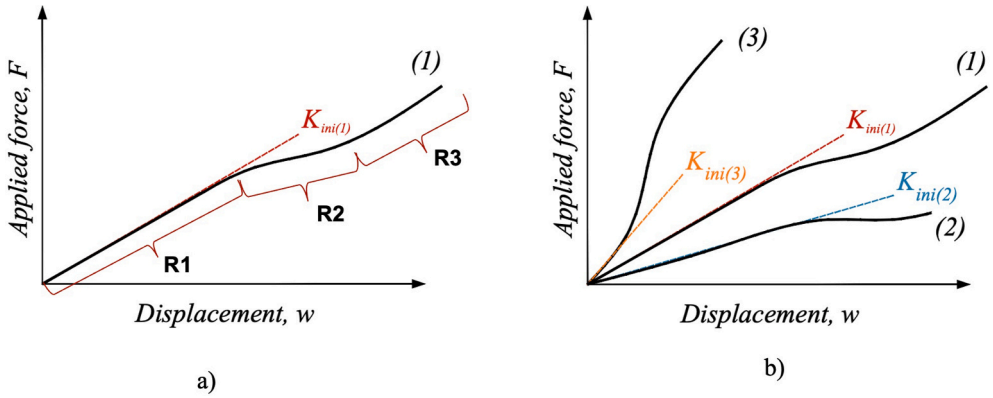

Fig. 2. Typical force-displacement curve on a web/face loaded out-of-plane.

[3–11].

An accurate design model for the initial elastic stiffness of the face plate component was recently proposed [1] that led to a simple analytical closed-form expression. However, establishing the design resistance requires the characterization of the full nonlinear force-displacement behaviour. Hence, firstly, the derivation of a practical solution for the large displacement response is required; secondly, it is necessary to establish appropriate criteria for the maximum strength level that can be achieved in a ductile way.

The objective of this paper is to contribute towards the development of a practical design formulation for the estimation of the design resistance of the face plate component that may be incorporated in design codes. This is achieved by first establishing an equivalent beam strip using the initial stiffness model presented in Conde *et al* [1]. Subsequently, the elastic large displacement solution for the equivalent beam strip subject to transverse loading is derived. Then, the large displacement model is extended to provide an elastic-plastic large displacement solution. Finally, a strain limit is used to establish the design load based on the Continuous Strength Method [12] as specified in Annex C of prEN 1993–1-14 [13].

2. Background

2.1. Scope

This section introduces the relevant background for the characterization of the design resistance of the face plate component. Firstly, the typical behaviour of this component is discussed in Section 2.2. This is extended by the existing literature studies which mostly addressed its initial stiffness, and plastic resistance. Conde *et al* [1] provided a thorough review of the initial stiffness and proposed an accurate model to predict it that is presented in Section 2.3. Concerning plastic resistance, most authors addressed the derivation of yield-line models. These are briefly reviewed in Section 2.4. Finally, the guidance for the establishment of the strain limits for resistance in Annex C of prEN 1993–1-14 [13] is summarized in section 2.5.

2.2. Behaviour of the face plate component

In the context of the joint typologies illustrated in Fig. 1, the typical force-deformation behaviour of the face plate component subjected to transverse forces is illustrated in Fig. 2a, depicting the following three regions [4,14]:

- Region 1, corresponding to small displacement plate bending, with an approximate linear response, characterized by the initial stiffness K_{ini}.
- Region 2, characterized by a progressive reduction of stiffness, due to yielding of steel.
- Region 3, characterized by re-stiffening of the force-deformation curve due to the progressive mobilization of membrane stiffness associated with large displacements.

Depending on the geometric properties of the face plate, several distinct behaviours may be observed, illustrated in Fig. 2b [15]. Case (1) was already described and exhibits relevant plasticity and membrane effects. Case (2) corresponds to a stocky plate whereby membrane effects are negligible (Region 3 is not identified); the resistance is controlled by plasticity and small displacement theory applies. In contrast, Case (3) corresponds to a slender plate which is controlled by membrane effects; in practical terms the influence of plasticity is negligible (Region 2 is not apparent) and large displacement theory is

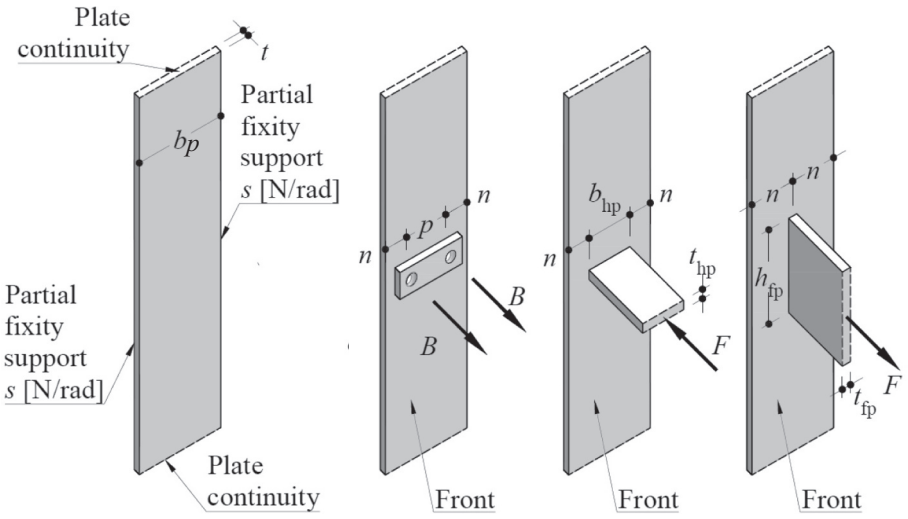

Fig. 3. Typical cases of connections to the web of an I section or the face of a tube (reproduced from [1]).

Table 1
Definition of geometric parameters.

	r	e	c
Bolt row in tension	2	$b_p/2$	d_m
Horizontal plate	2	$b_p/2$	$t + t_{hp}$
Vertical plate	1	b_p	h_{fp}

Table 2
Definition of stiffness coefficients.

	d_2	d_3
Bolt row in tension/ Horizontal plate	$\frac{n^3 s(2b-3n)+2EI_2 n^2(4n-3b)}{6EI_2(2EI_2+bs)}+\frac{n}{GA_v}$	$\frac{n^3}{12EI_2}\frac{sn+4EI_2}{sn+EI_2}+\frac{n}{GA_v}$
Vertical plate	$\frac{b^3(8EI_2+bs)}{192EI_2(2EI_2+bs)}+\frac{b}{4GA_v}$	$= d_2$

required.

Fig. 2 shows that either the load corresponding to the transition between Region 1 and Region 2 is too conservative to be taken as the design resistance of this component, or membrane forces (Region 3) appear before any significant yielding (Region 2). Classically, the knee of the force-deformation curve is taken as the resistance of steel components [16], either because it corresponds to full yielding of the component or because a buckling load is reached. This assumption is excessively conservative in this case [9,15] because:

(i) strain hardening is neglected, or for high strength steel grades or stainless steel, the uniaxial stress-strain behaviour of steel does not even exhibit a plastic plateau;
(ii) the plate mobilizes large membrane contributions and yielding under bending and axial stresses leads to higher plastic resistance than merely considering yielding in bending alone.

2.3. Initial stiffness

Concerning the initial stiffness of webs in I-sections or faces of RHS tubular sections loaded out-of-plane, most authors have proposed simplified expressions based on beam strip models, numerically calibrated for a specific range of validity. For end-plate joints directly attached to the column face, Neves and Gomes [3], proposed an expression for the initial stiffness of the column web in bending when subjected to an out-of-plane load applied on a rigid area that was derived using an equivalent strip model. Simões da Silva et al. [4] applied this model to assess the bending stiffness of the column face on tubular hollow sections filled with concrete in end-plate joints directly attached to the column face. Park and Wang [5] proposed a model based on the elastic solution of a plate loaded by point loads and other semi-empirical strip models have been proposed for the face of tubular columns [6–8]. More recently, Conde *et al* [1] proposed a new model to estimate the initial stiffness of the face plate component subjected to out-of-plane forces, based on a simplified grid in which a main beam in the face plate longitudinal direction is continuously supported by transverse beams. This model was validated against many FEM models, and it proved to be accurate in estimating the initial stiffness of this component. A practical closed-form solution was obtained using beam on elastic foundation theory, that can tackle horizontal or vertical plates connected perpendicularly to the face plate or bolts attached to the web/tube face, as depicted in Fig. 3. The initial stiffness of the face plate is given by:

$$K_{ini}^{CONDE} = r\left(8EI_1\lambda^3 + k_3 c\right) \tag{1}$$

where

$$\lambda = \sqrt[0.25]{\frac{k_3}{4EI_1}} \tag{2}$$

$$EI_2 = \frac{Et^3}{12(1-\nu^2)}\ EI_1 = eEI_2\ GA_v = \frac{2Gt}{3} \tag{3}$$

$$k_2 = \frac{1}{d_2}\ k_3 = \frac{1}{d_3} \tag{4}$$

Tables 1 and 2 show the definition of the geometrical parameters and the stiffness coefficients, respectively. E is the Young's modulus, ν is the Poisson's ratio, G is the shear modulus, b_p is the width of the face plate, t is the thickness of the face plate, t_{hp} is the thickness of the horizontal plate, t_{fp} is the thickness of the vertical plate, h_{fp} is de depth of the vertical plate, p is the bolt pitch and s is the rotational stiffness per unit length of the face plate longitudinal supports, A_v is the shear area of the rectangular cross-section.

Concerning the nonlinear behaviour, Neves and Gomes [3] proposed numerically fitted expressions for the membrane stiffness (K_m) that require the prior knowledge of the plastic resistance. However, Harada and Simões da Silva [9,10] showed that these equations provide poor results for many cases.

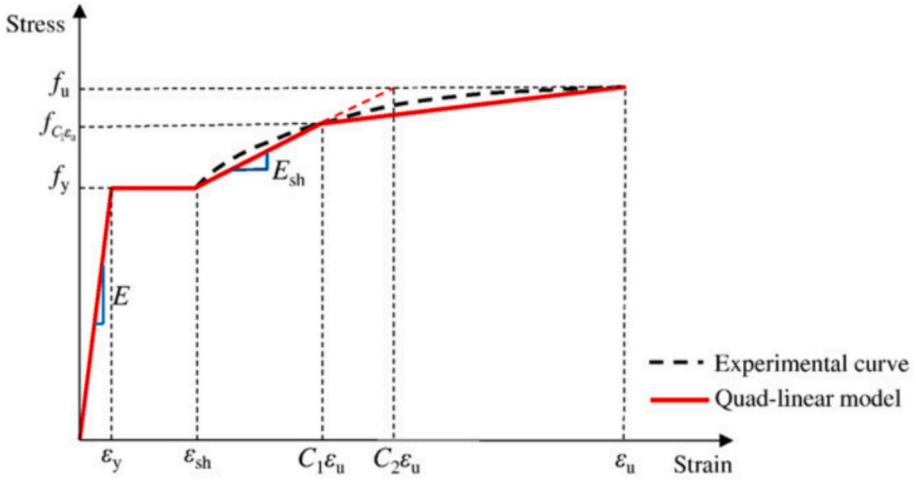

Fig. 4. Quadlinear Stress strain law (reproduced from [13]).

Table 3
Maximum design strains.

	Ω	$C_1\varepsilon_u/\varepsilon_y$	ε_{CSM} (%)
S235	15	56.6	1.7
S275	15	42.7	2.0
S355	15	32.2	2.5
S460	15	20.4	3.3

2.4. Plastic resistance

The evaluation of the plastic resistance of a column web/tube face loaded out-of-plane was mostly addressed using yield-line theory to derive design expressions. For longitudinal rectangular plates welded to the column face, Kosteski et al. [11] have proposed a design expression that is included in Eurocode 3, part 1–8 [2], henceforth denoted EC3–1-8. This equation was recently adopted [17] for a reverse channel welded to the column face, symmetrically placed with respect to the centerline of the column. For transverse rectangular plates welded to the column face or bolts attached to the column face through an endplate, several models are available: Wardenier et al. [18] that is adopted in EC3–1-8, the improved proposal by Gomes et al. [19], the simplified expressions by Yeomans [20] and BCSA/SCI [21] that is adjusted to deal with special fasteners such as Hollobolts and the recent proposal by Wang and Wang [22] that was experimentally calibrated to a set of 14 test results. The typical behaviour of the face component illustrated in Fig. 2 shows that very often it is difficult to identify the plastic resistance because of the development of membrane effects. Hence, for tubular joints, Zhao [23] proposed an empirical displacement-based resistance criterion (maximum out-of-plane deformation equal to 3% of the chord face width) that forms the basis of the calibration of many resistance expressions for tubular joints in EC3–1-8.

2.5. Strain limits

The resistance of the face plate subject to transverse loading corresponds to strains well above the yield strain and, in most cases, already in the large displacement range. The Continuous Strength Method (CSM) is "*a deformation-based approach to the design of structures that enables a continuous, rational and accurate allowance for material nonlinearity (i.e. the spread of plasticity and strain hardening)*" [12]. The method is applicable for defining cross-section failure in beam finite element models through the application of strain limits and was already incorporated in the forthcoming part 1–14 of Eurocode 3 [13]. Although the major objective of CSM is to incorporate the effects of local buckling, the method also provides guidance on the choice of the limiting strain under tensile conditions.

The CSM strain limit, ε_{csm}, that the cross-section can sustain prior to failure corresponds to the maximum longitudinal strain, and for non-slender cross-sections is given by [12]:

$$\frac{\varepsilon_{csm}}{\varepsilon_y} = \frac{0.25}{\overline{\lambda_p}^{3.6}} \text{ but } \frac{\varepsilon_{csm}}{\varepsilon_y} \le min\left(\Omega, \frac{C_1\varepsilon_u}{\varepsilon_y}\right) \text{ for } \overline{\lambda_p} \le 0.68 \tag{5}$$

where ε_y is the yield strain, ε_u is the ultimate strain, $\overline{\lambda_p}$ is the cross-sectional slenderness used to assess the susceptibility to local instability, Ω is the maximum level of plastic strain, and C_1 is a coefficient corresponding to the adopted CSM material model. In this case, only the second condition applies.

Hence it, is required to specify an appropriate stress-strain curve for steel. The quad-linear material model proposed by Yun and Gardner [24] provides a simple and accurate representation of the elastic, yield plateau and strain hardening characteristics of hot-rolled steels. It is given in eqs. (6) to (11) and is illustrated in Fig. 4:

$$\sigma = \begin{cases} E\varepsilon & for\ \varepsilon \le \varepsilon_y \\ f_y & for\ \varepsilon_y < \varepsilon \le \varepsilon_{sh} \\ f_y + E_{sh}(\varepsilon - \varepsilon_{sh}) & for\ \varepsilon_{sh} < \varepsilon \le C_1\varepsilon_u \\ f_{C_1\varepsilon_u} + \dfrac{f_u - f_{C_1\varepsilon_u}}{\varepsilon_u - C_1\varepsilon_u}(\varepsilon - C_1\varepsilon_u) & for\ C_1\varepsilon_u < \varepsilon \le \varepsilon_u \end{cases} \tag{6}$$

with

$$\varepsilon_{sh} = 0.1\frac{f_y}{f_u} - 0.055, \text{but } 0.015 \le \varepsilon_{sh} \le 0.03 \tag{7}$$

$$\varepsilon_u = 0.6\left(1 - \frac{f_y}{f_u}\right), \text{but } \varepsilon_u \ge 0.06 \tag{8}$$

$$C_1 = \frac{\varepsilon_{sh} + 0.25(\varepsilon_u - \varepsilon_{sh})}{\varepsilon_u} \tag{9}$$

$$C_2 = \frac{\varepsilon_{sh} + 0.4(\varepsilon_u - \varepsilon_{sh})}{\varepsilon_u} \tag{10}$$

and, for hot-rolled carbon steels,

$$E_{sh} = \frac{f_u - f_y}{C_2\varepsilon_u - \varepsilon_{sh}} \tag{11}$$

Hence, for steel grades S235 to S460, this leads to the maximum design strains of Table 3:

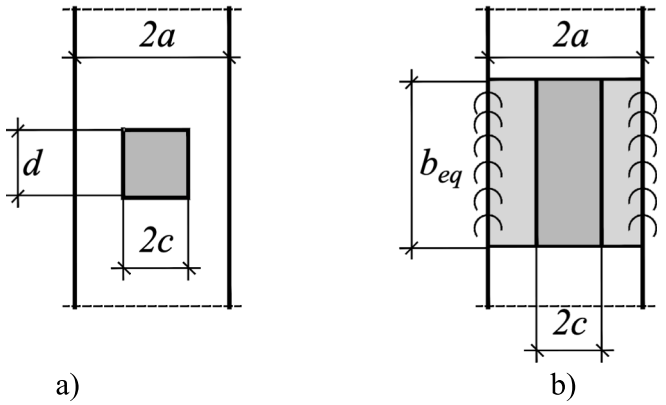

Fig. 5. Definition of the equivalent beam strip: a) real plate subject to patch loading; b) equivalent beam strip.

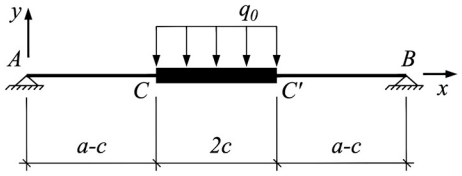

Fig. 6. Nonlinear beam strip model.

3. Mechanical model for the large displacement behaviour of the face plate

3.1. Description of the model

Fig. 5a illustrates the face plate component, corresponding to the generic case of the web of a I-section or the face of a RHS profile subject to an out-of-plane force due to a group of bolts or a horizontal or a vertical plate (flange of a I-section or a fin plate). This component behaves as a plate with a central patch load with dimensions *2c* x *d*, with an infinite length and a width *2a* that approximately corresponds to the distance between flanges in case of an I-section or the distance between the side-faces in case of a tubular cross-section [15]. The longitudinal boundary conditions correspond to flexible rotational supports with stiffness *s* per unit length, representing the restraining effect of the flanges or the side faces of a tubular profile.

The main assumption for the proposed mechanical model for the large displacement behaviour of the face plate component is illustrated in Fig. 5b and corresponds to the consideration of a beam strip with an equivalent width b_{eq}. The width b_{eq} is established by equating the initial stiffness of the equivalent grid model proposed in [1], given by eq. (1), to the linear elastic stiffness of the beam strip, obtained as explained in section 3.2. The span of the beam strip is taken as *2a* and the patch load is applied on a central segment spanning the full width b_{eq} of the beam. Finally, the side segments of the beam strip have the same thickness *t* as the original plate and the thickness of the central segment where the patch load is applied, t_2, depends on the detail of the connecting element that transfers to out-of-plane force (group of bolts or a horizontal or a vertical plate).

It is useful to define the non-dimensional parameters α, β, μ, as follows:

$$\alpha = \frac{d}{b_{eq}}\ \beta = \frac{c}{a}\ \mu = \frac{2a}{t}. \tag{12}$$

Subsequently, the equivalent beam strip is used to derive a large displacement solution. This derivation is shown in detail in Section 3.2 for the elastic large displacement solution and in Section 3.3 for the elastic-plastic large displacement solution.

The final step corresponds to the establishment of the design resistance of the component. This is obtained using the uniaxial material model from eqs. (6) to (11) or an alternative appropriate material model that includes straight hardening, by introducing the CSM strain limit obtained directly from Table 3 in the elastic-plastic large displacement force-strain curve, as explained in Section 3.4.

3.2. Derivation of the large displacement equations

3.2.1. Simply-supported beam strip

Consider the simply supported beam with a rectangular cross section of width *b*, thickness *t* in the side segments and t_2 in the middle segment, illustrated in Fig. 6, subject to a patch load q_0, where the axial displacement is restrained.

From equilibrium, the bending moment is given by:

$$M(x) = \begin{cases} q_0 cx & x < a-c \\ q_0 cx - q_0 \dfrac{(x-a+c)^2}{2} & a-c < x < a+c \\ q_0 cx - 2q_0 c(x-a) & a+c < x < 2a \end{cases} \tag{13}$$

The solution is obtained using an energy formulation and the Rayleigh-Ritz method [25]. The total potential energy *V* is given by:

$$\begin{aligned} V =& \frac{1}{2}\int_0^{a-c}\left(EI\left(\frac{\partial^2 w}{\partial x^2}\right)^2 + EA\left(\frac{\partial u}{\partial x}+\frac{1}{2}\left(\frac{\partial w}{\partial x}\right)^2\right)^2\right)dx \\ &+\frac{1}{2}\int_{a-c}^{a+c}\left(EI_2\left(\frac{\partial^2 w}{\partial x^2}\right)^2 + EA_2\left(\frac{\partial u}{\partial x}+\frac{1}{2}\left(\frac{\partial w}{\partial x}\right)^2\right)^2\right)dx \\ &+\frac{1}{2}\int_{a+c}^{2a}\left(EI\left(\frac{\partial^2 w}{\partial x^2}\right)^2 + EA\left(\frac{\partial u}{\partial x}+\frac{1}{2}\left(\frac{\partial w}{\partial x}\right)^2\right)^2\right)dx + \int_{a-c}^{a+c} q_0 w dx \end{aligned} \tag{14}$$

where *u* is the longitudinal displacement in the x-direction and *w* represents the transverse displacement in the y-direction. Three displacement functions were adopted w_1 corresponding to the region AC, w_2 to CC' and w_3 to C'B. The boundary conditions are:

$$\begin{aligned} &w_1(0) = w_3(2a) = 0 \\ &w_1(a-c) = w_2(a-c) = 0 \\ &w_1'(a-c) = w_2'(a-c) = 0 \\ &w_3(a+c) = w_2(a+c) = 0 \\ &w_3'(a+c) = w_2'(a+c) = 0 \end{aligned} \tag{15}$$

w' denotes the first derivative of the transverse displacement with respect to x ($w' = dw/dx$).

Assuming the following displacement function for the transverse displacement *w*, that corresponds to the solution of the small displacement differential equation for the beam strip,

$$w(x) = \begin{cases} w_{mn}\dfrac{cx}{6EI}\left(3(a-c)^2 - x^2 + \dfrac{2I}{I_2}(3ac-2c^2)\right) \\ w_{mn}\left(\dfrac{x\left(x^3-4ax^2+6(a-c)^2x-4a^3-12ac^2+24a^2c\right)}{24EI_2} - \dfrac{a^4+9c^4+30a^2c^2-28ac^3-12a^3c}{24EI_2} - \dfrac{c(a-c)^3}{3EI}\right) \\ -w_{mn}\dfrac{c(2a-x)(a^2-3ac^2+4I/c^2I_2+x^2+6ac-4ax-6I/acI_2)}{6EI} \end{cases} \tag{16}$$

where w_{mn} is the amplitude of the transverse displacement *w*, *I* and I_2

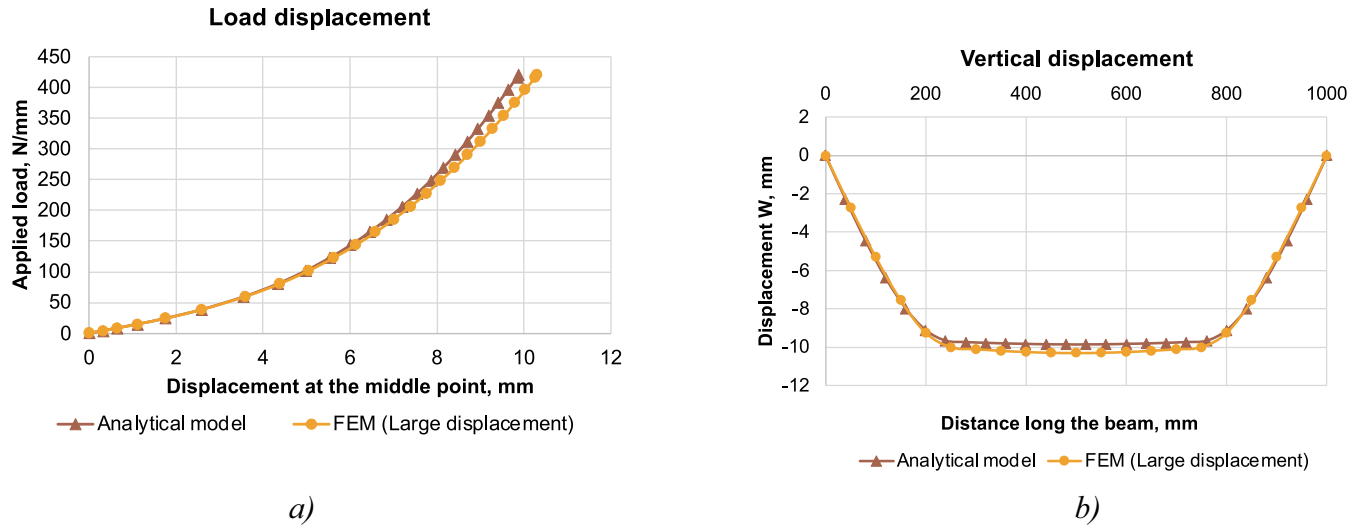

Fig. 7. Comparison of numerical and analytical results: (a) transverse force-displacement curve at point C; (b) variation of transverse displacements with beam length.

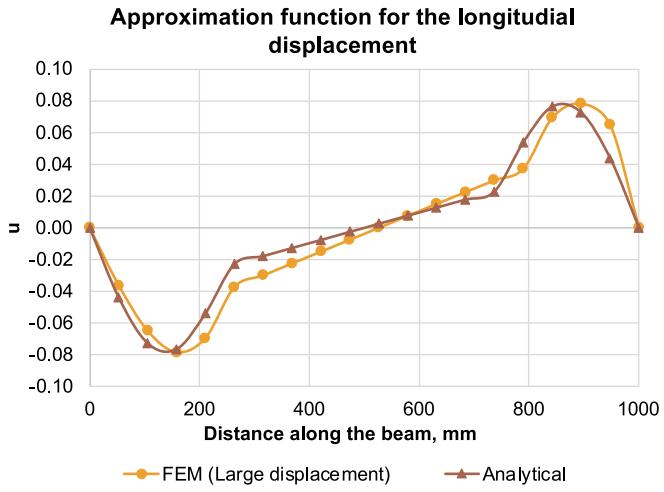

Fig. 8. Comparison of numerical and analytical axial displacements.

are the moments of inertia of the beam strip along the segments AC and C'B and CC', respectively, and the axial displacement u given by

$$u(x) = \begin{cases} -u_{mn} sin\dfrac{0.9\pi x}{a-c} & for\ x < a-c \\ -u_{mn}\dfrac{x-a}{c} sin 0.9\pi & for\ a-c < x < a+c \\ u_{mn} sin\dfrac{0.9\pi(2a-x)}{a-c} & for\ a+c < x < 2a \end{cases} \tag{17}$$

where u_{mn} is the amplitude of the longitudinal displacement u, the application of the Rayleigh-Ritz method leads to the following system of algebraic equations:

$$\frac{\partial V}{\partial u_{mn}} = 0 \tag{18a}$$

$$\frac{\partial V}{\partial w_{mn}} = 0 \tag{18b}$$

Solving eq. (18a) for u_{mn} gives

$$u_{mn} = \bar{u} w_{mn}^2 \tag{19}$$

and replacing u_{mn} in eq. (18b) yields:

$$A_1 w_{mn}^3 + B_1 w_{mn} - B_1 q_0 = 0 \tag{20}$$

Solving eq. (20) for w_{mn} yields:

$$w_{mn} = -2\sqrt{\frac{p_1}{3}} sinh\left[\frac{1}{3} sinh^{-1}\left(\frac{3q_1}{2p_1}\sqrt{\frac{3}{p_1}}\right)\right] \tag{21}$$

with

$$p_1 = \frac{B_1}{A_1} \text{ and } q_1 = -\frac{B_1 q_0}{A_1}. \tag{22}$$

Eqs. (23) and (24) that define the constants $\bar{u}$, A_1 and B_1 were obtained through symbolic manipulation using MATLAB [26]. The corresponding solution is henceforth denoted "exact". Because these expressions are too long for practical application in a quick calculation or for inclusion in a code of practice, they can be simplified assuming that I_2 is higher compared to I, leading to:

$$\bar{u} = \frac{104.13 A c^3 (a-c)^5}{\pi^4 E^2 I^2 [Ac\pi(4.24\pi - 1.38) + A_2(a-c)\ ]} \tag{23}$$

$$A_1 = 1944 A\pi^4 c^2 (a-c)^6 - 3044439.39 \bar{u} A E^2 I^2 (a-c) \tag{24a}$$

$$B_1 = 51030\pi^4 E^2 I^3 \tag{24b}$$

The corresponding solution is henceforth denoted "rigid". In case of small displacements, $w_{mn} = q_0$, and the elastic stiffness of the simply supported beam strip is obtained by dividing the applied load q_0 by the corresponding maximum displacement w (eq. 16) at cross section C or C′, yielding:

$$K_{el} = \frac{6EI}{(a-c)^2 + \frac{I}{I_2} c(3a-2c)} \frac{a}{c(a-c)} \tag{25}$$

Eq. (25) allows to calculate the width b_{eq} of the equivalent beam strip as follows:

$$b_{eq} = \frac{2c(a-c)}{Eat^3}\left[(a-c)^2 + \frac{I}{I_2} c(3a-2c)\right] K_{ini}^{CONDE} \tag{26}$$

3.2.2. *Validation of assumed displacement functions*

Considering, for exemplification, a simply supported beam strip (see Fig. 6) with length $2a = 500$ mm, thickness $t = 10$ mm, width $b = 1000$ mm, loaded with a uniformly distributed load q_0 over a central segment

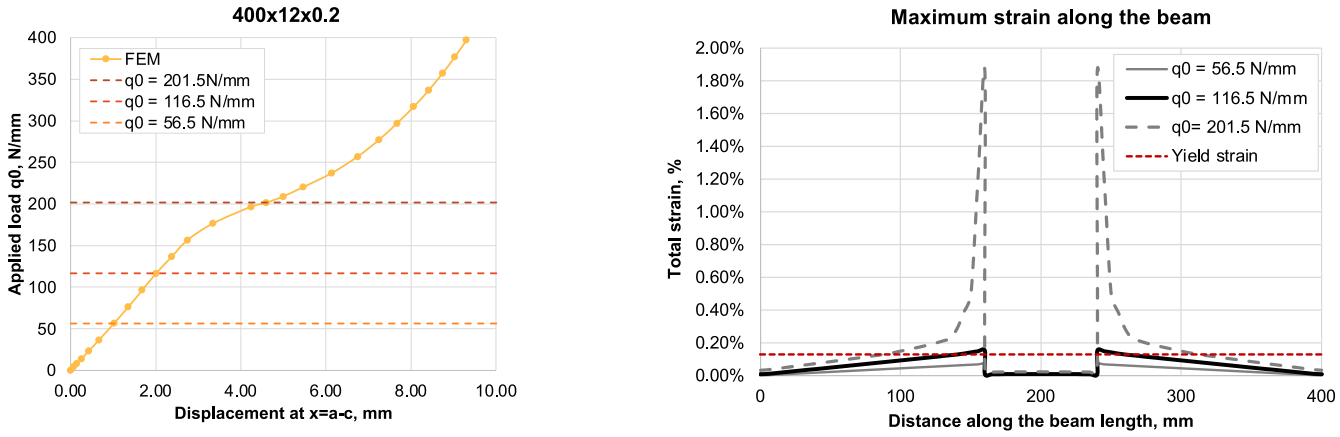

a) b)

Fig. 9. FEM results for beam strip: a) Load displacement curve; b) Variation of longitudinal strain along the beam.

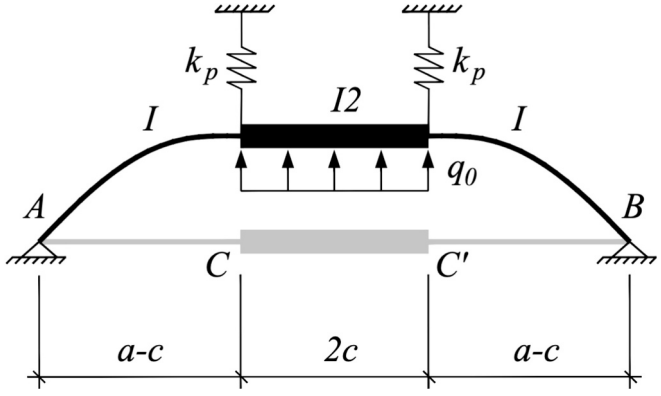

Fig. 10. Lumped plasticity beam strip model.

of length $2c = 250$ mm and with $I_2 = 64I$, where I is the moment of inertia of the side segments, Fig. 7a compares the elastic large displacement numerical solution obtained using the FEM software ABAQUS [27] using beam elements and the analytical solutions given by eq. (16), showing a perfect match. Fig. 7b compares the transverse displacements along the length of the beam strip for a load level of 420 N/mm, again showing a perfect match.

Fig. 8 compares the numerical (ABAQUS) and the analytical (eq. (17)) axial displacements, showing good agreement.

Similar agreement is obtained for all the cases that were examined in the parametric study, defined later in Section 4.

3.2.3. *General solution for arbitrary boundary conditions*

The web to flange junction of a I-section or the corner of a tubular cross-section provides a partial rotational restraint, s, to the supports of the equivalent beam strip. Given appropriate displacement functions $w(x)$ and $u(x)$, it is possible to repeat the derivation shown in sub-Section 3.2.1, considering the appropriate rotational boundary conditions at its ends. This leads to the generic large displacement elastic solution, given by:

$$w_{el}^{LD}(x) = w_{mn} f(x, a, c, E, A, A_2, I, I_2, s). \tag{27}$$

3.3. *Derivation of the elastic-plastic large displacement equations*

The elastic-plastic behaviour of the beam strip of Fig. 6 shows that plasticity first occurs at the transition between the deformable segments with stiffness EI and the much more rigid central segment where the patch load is applied. Fig. 9 illustrates the force-displacement curve (Fig. 9a) and strain contours (Fig. 9b) along the length and across the thickness of a beam strip, with dimensions $2a = 400$ mm, $2c = 80$ mm, $t = 12$ mm and $b = 100$ mm in steel S275, showing clearly that the plasticity is concentrated at the transitions between the central rigid segment and the side segments.

Hence, it is reasonable to consider a lumped plasticity assumption such that the limiting strain occurs at points C and C′. Using the analogy of an equivalent post-buckling elastic model to mimic the plastic behaviour at those cross-sections that was successfully employed in the context of steel connections [28], the model of Fig. 10 is proposed.

It adds the two springs with stiffness k_p, that represent the plasticity at these cross sections, leading to:

$$w_{el-pl}^{LD}(x) = w_{el}^{LD}(x) + \frac{1}{k_p}\left(q_0 - q_p\right) \tag{28}$$

where k_p is the plastic stiffness of cross-sections C and C′, q_p is the load corresponding to the plastic moment resistance at these cross-sections and w_{el}^{LD} was derived in the previous section.

In case of small displacements, q_p is obtained directly from eq. (29):

$$q_p = \frac{bt^2 f_y}{4c(a-c)} \tag{29}$$

while the load corresponding to the elastic moment is also given by eq. (29) by replacing 4 by 6. However, in the presence of membranes strains, these must be accounted for in the calculation of $q_{p\cdot}$, as the axial force influences the moment-curvature relations [29]. The strain at a generic point of the beam for the first branch of the beam strip is given by the following expression, considering membrane and bending strains and neglecting the second term:

$$\varepsilon(x,z) = \frac{du(x)}{dx} + \frac{1}{2}\left(\frac{dw(x)}{dx}\right)^2 \pm z\frac{d^2w(x)}{dx^2} \approx \frac{0.9\pi}{a-c}u_{mn}cos\frac{0.9\pi x}{a-c} \pm \frac{cxz}{EI}w_{mn} \tag{30}$$

The plastic load modified by the membrane strains, $q_{y,m}$, is obtained by equating eq. (30) to the plastic strain at the transition between the central stiffer segment and the side segments,

$$\varepsilon\left(a-c,\, t/2\right) = \frac{2.689}{a-c}\bar{u}w_{mn}^2 \pm \frac{c(a-c)t}{2EI}w_{mn} = \varepsilon_{sh} \tag{31}$$

and solving for the force q_0.

The plastic membrane stiffness, k_p, is obtained as the stiffness of cross sections C and C′ considering strain hardening, *i.e.*, assuming that these plastic hinges are operating in the range $\varepsilon_{sh} < \varepsilon \leq C_1\varepsilon_u$ (see eqs. (6)),

Table 4
Parametric study.

	Values	No cases
2a (mm)	100, 150, 200, 250, 300, 400, 500, 600, 750, 900	10
t (mm)	4, 6, 8, 10, 12	5
$\beta = c/a$	0.1, 0.2, 0.3, 0.4, 0.5, 0.6	6

Table 5
Statistical characterization of the error Δ_i of the analytical large displacement elastic solution.

	$\beta =$ **0.1**	$\beta =$ **0.2**	$\beta =$ **0.3**	$\beta =$ **0.4**	$\beta =$ **0.5**	$\beta =$ **0.6**	**All**
mean	0.971	0.990	0.997	0.999	0.996	0.990	**0.991**
stdev	0.011	0.005	0.008	0.012	0.016	0.016	**0.016**
C.o. V.	1.1%	0.5%	0.8%	1.2%	1.6%	1.6%	**1.7%**
min	0.949	0.972	0.964	0.952	0.952	0.903	**0.903**
max	0.984	0.995	1.002	1.008	1.008	1.014	**1.014**

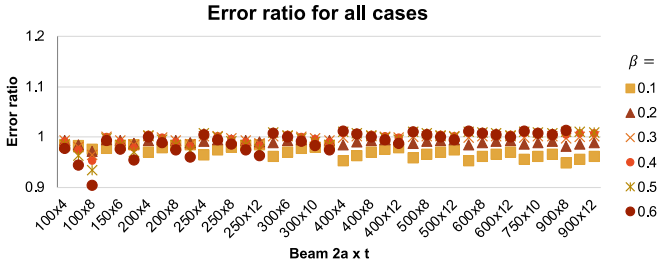

Fig. 11. Error ratio Δ_i for all cases.

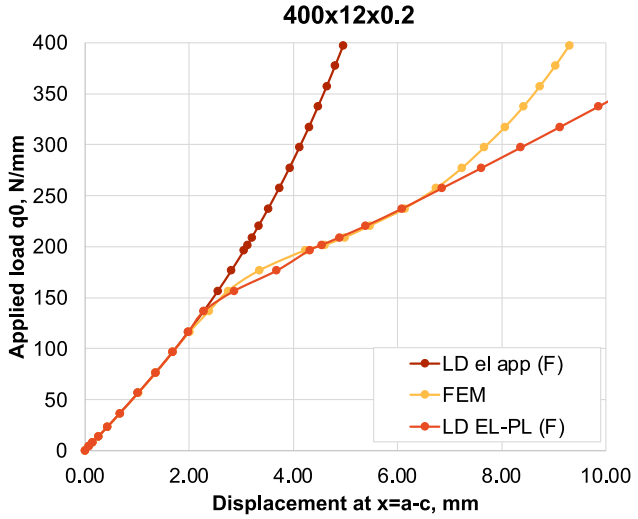

Fig. 12. Comparison between FEM results and analytical model (exact and rigid approximation) for beam 400 × 12 × 0.2.

leading to:

$$k_p = \alpha_p \frac{E_{sh}}{(a-c)^2}\frac{bt^3}{12} \tag{32}$$

where α_p is a plastic correction factor that was numerically calibrated with the results of the parametric study described in section 4.

$$\alpha_p = 0.0881\mu\left(\beta t^2\right)^{-1.04} - 0.9\left(\beta t^2\right)^{-0.889} \tag{33}$$

Table 6
Validation of the large displacement elastic-plastic model.

	$\beta =$ **0.1**	$\beta =$ **0.2**	$\beta =$ **0.3**	$\beta =$ **0.4**	$\beta =$ **0.5**	$\beta =$ **0.6**	**All**
mean	0.995	0.992	1.006	0.996	0.990	1.011	**0.998**
stdev	0.023	0.023	0.031	0.041	0.034	0.034	**0.003**
C.o. V.	2.3%	2.3%	3.0%	4.1%	3.4%	3.3%	**3.3%**
min	0.954	0.936	0.923	0.930	0.930	0.899	**0.899**
max	1.087	1.030	1.093	1.172	1.172	1.108	**1.172**

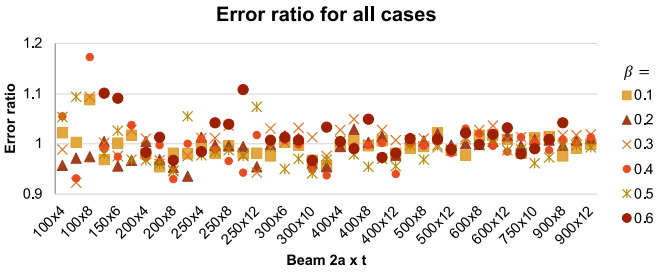

Fig. 13. Error ratio for all cases.

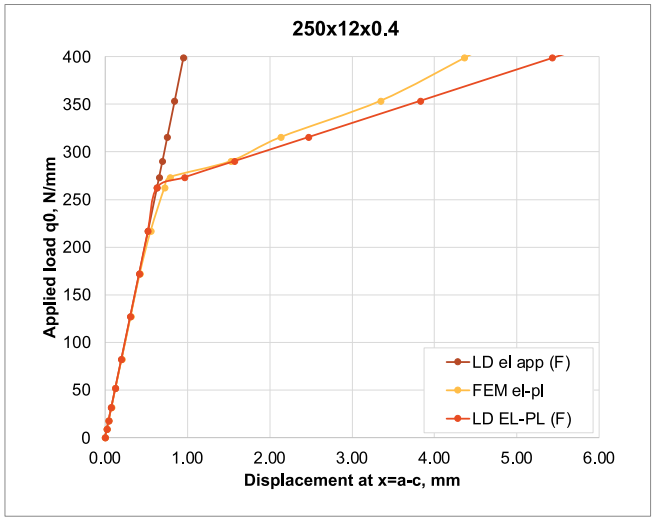

Fig. 14. Comparison between FEM results and analytical model for beam.

3.4. Design resistance

According to the qualitative behaviour of the face plate component illustrated in Fig. 2, the design resistance is reached whenever one of the following two conditions is met:

- A limiting maximum strain is reached.
- A maximum deformation is reached.

Using the proposed equivalent beam strip model with the CSM strain limits defined in Table 3 and the 3% deformation limit described in section 2.2, the design resistance is given by:

$$F_{Rd} = min\begin{cases} \varepsilon_{tot}^{max} = \varepsilon_{CSM} \\ w_{el-pl}^{LD} = 0.03b \end{cases} \tag{34a, b}$$

Considering the second criterion, F_{Rd} is directly obtained from eq. (34b) by solving eq. (28) with respect to q_0. Concerning eq. (34a), assuming first that membrane effects are negligible (Case 2 in Fig. 2), small displacements apply and q_{CSM} is obtained directly from the elastic-

Fig. 15. Vertical displacements for load levels q_y and q_{CSM}.

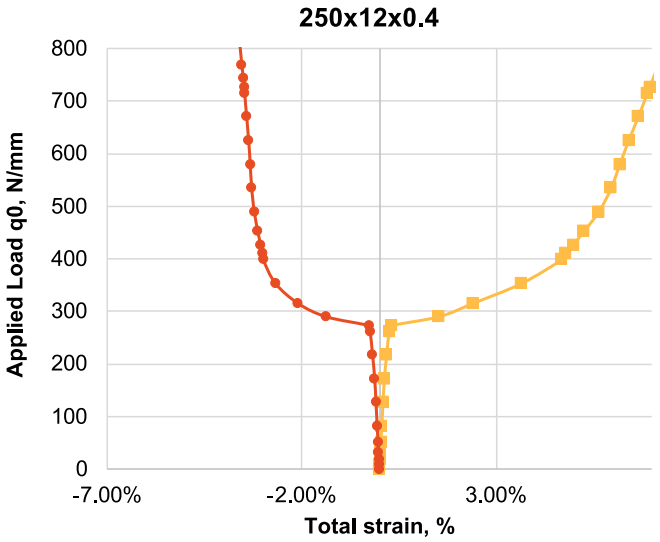

Fig. 16. Total top and bottom strain at point C.

plastic behaviour of cross-sections C or C′, from the total bending strains (ε_b) and the corresponding moment-curvature relations for the quad-linear material model of Fig. 4 at point C or C′, as described in the following paragraphs.

Firstly, the bending strain is related to the curvature according to eq. (35)

$$\chi = \frac{2\varepsilon_b}{t} \tag{35}$$

Secondly, the corresponding moment-curvature relations are given by [30]:

For $\frac{\chi}{\chi_y} \leq 1$

$$\frac{M}{M_y} = \frac{\chi}{\chi_y} \tag{36}$$

where M_y is the elastic moment of cross-section C and χ_y is the curvature corresponding to first yield, given by:

$$M_y = \frac{bt^2}{6} f_y \tag{37}$$

$$\chi_y = \frac{2\varepsilon_y}{t} \tag{38}$$

For $1 < \frac{\chi}{\chi_y} \leq \frac{\chi_{sh}}{\chi_y}$

$$\frac{M}{M_y} = \frac{1}{2}\left[3 - \left(\frac{\chi_y}{\chi}\right)^2\right] \tag{39}$$

where χ_{sh} is the curvature corresponding to the end of the yield plateau (see Fig. 4, ε_{sh}), given by:

$$\chi_{sh} = \frac{2\varepsilon_{sh}}{t} \tag{40}$$

For $\frac{\chi_{sh}}{\chi_y} < \frac{\chi}{\chi_y} \leq \frac{\chi_{C1}}{\chi_y}$

$$\frac{M}{M_y} = \frac{1}{2}\left[3 - \left(\frac{\chi_y}{\chi}\right)^2\right] + \frac{1}{2}\frac{E_{sh}}{E}\left(\frac{\chi - \chi_{sh}}{\chi_y}\right)\left(1 - \frac{\chi_{sh}}{\chi}\right)\left(2 + \frac{\chi_{sh}}{\chi}\right) \tag{41}$$

where E_{sh} is defined in eq. (11) and $\chi_{C1\varepsilon u}$ is the curvature corresponding to strain $\varepsilon_{C1\varepsilon u}$ (see Fig. 4), given by:

$$\chi_{C1\varepsilon u} = \frac{2\varepsilon_{C1\varepsilon u}}{t} \tag{42}$$

Hence, since

$$M^C = q_0 c(a - c) \tag{43}$$

and introducing eqs. (35) and (43) into eq. (41) yields:

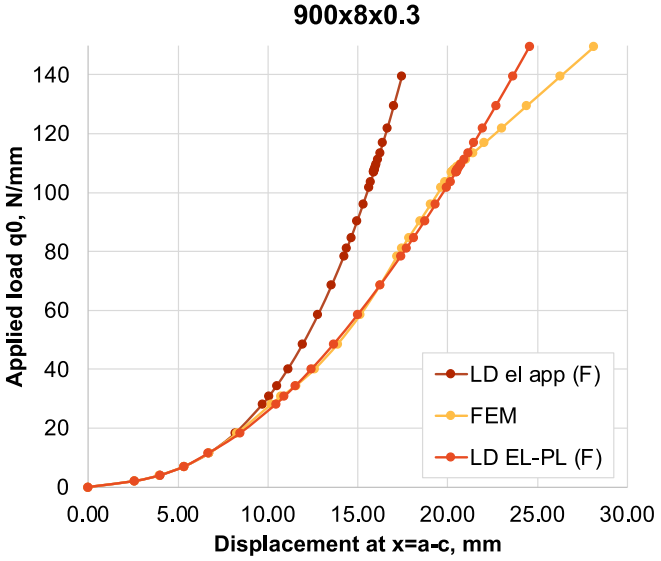

Fig. 17. Comparison between FEM results and analytical model for beam.

Table 7
Detailed results at specific load levels.

Load level	q_{el}^{SD} N/mm	q_{el}^{LD} N/mm	$q_{el\text{-}pl}^{LD}$ N/mm	w_{el}^{SD} mm	w_{el}^{LD} mm	$w_{el\text{-}pl}^{LD}$ mm	$\varepsilon_t^{el\text{-}pl}$ %	$\varepsilon_b^{el\text{-}pl}$ %
q_y	176.0	180.2	176.7	0.42	0.44	0.44	0.131	0.127
q_p	264.0	2466.2	291.0	0.64	4.52	1.54	1.551	−1.387
q_{CSM}	264.6	3367.4	302.9	0.64	5.50	1.83	1.964	−1.728

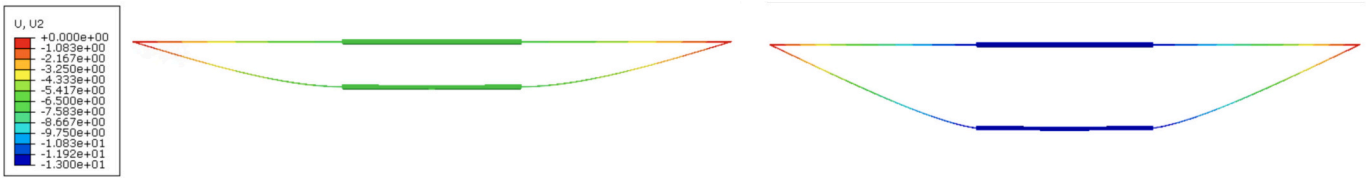

Fig. 18. Vertical displacements for load levels qy and qCSM.

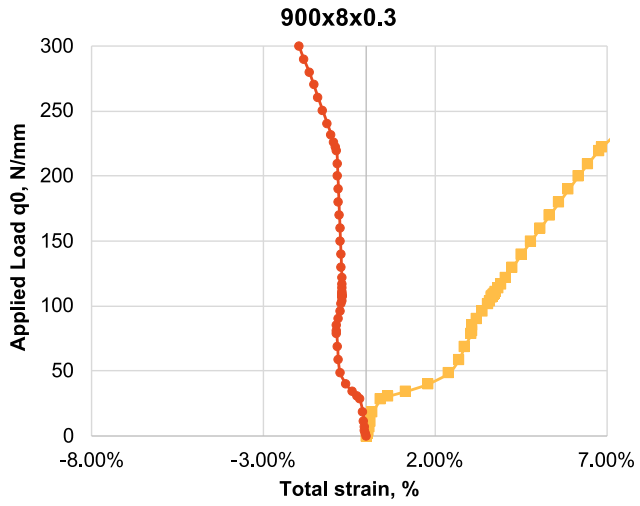

Fig. 19. Total top and bottom strain at point C.

$$q_{0,CSM}^{SD} = \frac{1}{2c(a-c)} M_y \left[\left[3 - \left(\frac{t\chi_y}{2\varepsilon_{CSM}} \right)^2 \right] + \frac{E_{sh}}{E} \left(\frac{2\varepsilon_{bCSM} - t\chi_{sh}}{t\chi_y} \right) \left(1 - \frac{\chi t_{sh}}{2\varepsilon_{CSM}} \right) \left(2 + \frac{t\chi_{sh}}{2\varepsilon_{CSM}} \right) \right] \tag{44}$$

For the more general case of relevant membrane effects (cases 1 and 3), according to the equivalent post-buckling elastic model of Fig. 10, the total strain is obtained by superimposing the bending and membrane strains resulting from the elastic large displacement solution w_{el}^{LD} and the localized plastic bending strains modified by axial force occurring at the equivalent plastic hinges. The design resistance is obtained by solving the resulting total strain with respect to q_0.

4. Validation

4.1. Methodology

4.1.1. Scope

The validation of the nonlinear equivalent beam strip model is carried out by comparison with nonlinear numerical models implemented in the FEM software ABAQUS. This validation is carried out in two steps. Firstly, the analytical solutions for the elastic large displacement solutions of the beam strip illustrated in Fig. 6 are compared to the numerical results obtained using ABAQUS from a geometrically nonlinear analysis using beam elements to validate the assumed displacement fields in the Rayleigh-Ritz analysis. Secondly, a parametric study is carried out to compare the numerical results obtained using ABAQUS for the elastic-plastic large displacement response with the analytical methodology proposed in this paper.

4.1.2. Numerical model

The numerical model was implemented using 2-node linear beam elements B31. The supports at the beam extremities restrain vertical and axial displacements. A fine mesh with a 5 mm maximum element size was adopted.

For all beams two types of analyses were performed: i) large displacement elastic analysis and ii) large displacement elastic-plastic analysis with the material model presented in section 2.5. The steel grade for all models was S275.

4.2. Validation of the proposed model

4.2.1. Parametric study

A parametric study is implemented, covering a practical range of geometries of webs of I-beams and faces of tubular columns. Table 4 lists the parameters considered in the parametric study and the corresponding range of values, totaling 273 distinct cases in steel grade S275 and a constant beam width of $b = 100$ mm.

4.2.2. Large displacement elastic solution

The large displacement elastic solution from the numerical model is

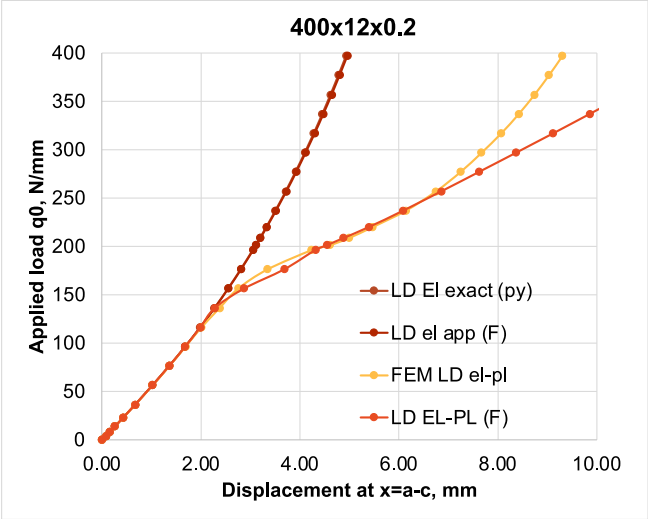

Fig. 20. Comparison between FEM results and analytical model for beam.

Table 8
Detailed results at specific load levels.

Load level	q_{el}^{SD}	q_{el}^{LD}	$q_{el\text{-}pl}^{LD}$	w_{el}^{SD}	w_{el}^{LD}	$w_{el\text{-}pl}^{LD}$	ε_t	ε_b
q_y	6.9	13.1	12.7	7.1	7.1	7.0	0.131	−0.078
q_p	10.35	661.7	38.0	16.62	31.9	12.2	1.551	−0.53
q_{CSM}	10.37	985.0	42.6	16.65	36.7	13.0	1.964	−0.647

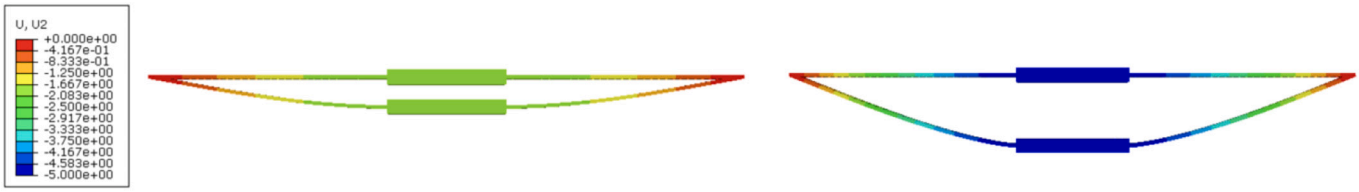

Fig. 21. Vertical displacements for load levels qy and qCSM.

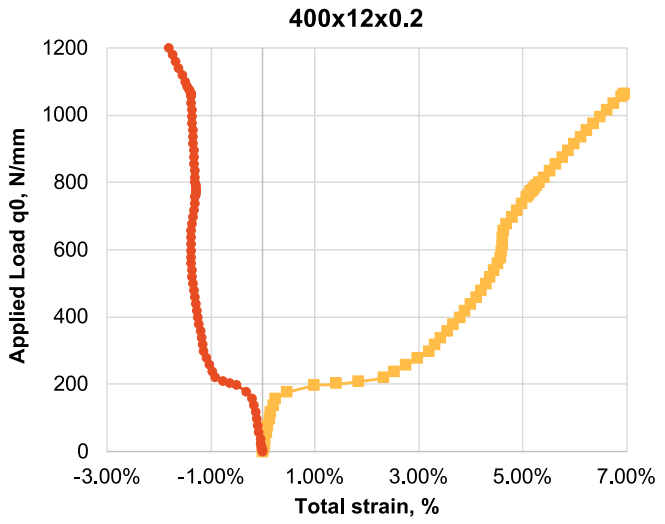

Fig. 22. Total top and bottom strain at point C.

compared to the analytical model for each beam and β ratio. The error Δ_i is calculated according to eq. (45) as the ratio of the analytical elastic large-displacement, $w_{el,i}^{LD}$, obtained using eq. (16), and the numerical elastic large displacement, $w_{FEM,i}^{LD}$, given by the finite element results, at cross section C, averaged over the number of load increments, from the origin until load increment *ninc*, corresponding to a load five times the yield load of each beam:

$$\Delta_i = \frac{1}{ninc}\sum_{1}^{ninc}\frac{w_{el,i}^{LD}}{w_{FEM,i}^{LD}} \tag{45}$$

The average values of the error ratio for all beams and β ratios are presented in **Table 5** and Fig. 11, together with their variation (standard deviation (stdev) and coefficient of variation (C.o.V.)) and min and max values, showing excellent agreement.

For exemplification, Fig. 12 compares the large displacement elastic results obtained from FEM (FEM LD el) with the analytical model (LD EL exact) and (LD EL rigid) for the example defined in section 3.3. The three lines are exactly superimposed, showing the accuracy of the analytical solutions.

4.2.3. Large displacement elastic-plastic solution

The large displacement elastic-plastic solution is evaluated at point C (see Fig. 6), where the cross-section changes and for loads which cause strain between the yield strain and the 2% strain. For each load increment in the numerical model, the corresponding displacement w_{el-pl}^{LD} was calculated. Then the ratio between the analytical and numerical values was computed for each point between the yield load and 2% plastic strain load. The average values of this ratio for all models are presented in **Table 6** and Fig. 13, together with its valuation showing very good agreement except for some cases with higher β value (0.5 and 0.6). Fig. 11 compares the large displacement elastic-plastic results obtained from FEM (FEM LD el-pl) with the analytical model (LD el-pl) for the example defined in section 3.3. The agreement is very good until a displacement of 7 mm, corresponding to a total strain of $\varepsilon = 3\%$, well beyond the design strain, showing the accuracy of the analytical solutions. (See Fig. 14.)

5. Discussion

Having derived accurate analytical solutions for the large-displacement elastic and elastic-plastic response of a beam strip representing the face plate of the column web of a I-section or the face of a tubular column loaded out-of-plane, the three typical behaviours described in section 1 are now discussed in detail using illustrative examples.

5.1. Stocky beam strip

Consider a simply supported beam strip (see Fig. 6) with length $2a = 250$ mm, thickness $t = 12$ mm, width $b = 100$ mm, loaded with a uniformly distributed load q_0 over a central segment of length $2c = 100$ mm and with $I_2 = 64I$ and $A_2 = 4A$, where I is the moment of inertia and A is the area of the side segments. Fig. 7 depicts the linear elastic solution, large displacement elastic solution and large displacement elastic-plastic solution, all calculated numerically using ABAQUS and applying the analytical equations derived in section 3. Firstly, the first order solution (linear elastic) is almost perfectly superimposed with the large displacement elastic solution, showing that membrane effects are not relevant for this example (Case 2). Secondly, the numerical elastic-plastic curve is well approximated by the analytical solution.

Fig. 15 compares the deformed shape for two load levels: load q_p corresponding to the plastic resistance of cross-section C and load q_{CSM} corresponding to the strain ε_{CSM} at the same cross-section.

Fig. 16 illustrates the variation of the total top and bottom strain at point C, showing that there is a marked plastic plateau already exhibiting membrane strains as yielding occurs.

The deformation criterion (7.5 mm) given by eq. (34b) leads to a maximum resistance of 462.5 N/mm. Table 7 summarizes relevant results for practical application for three load levels (q_y, q_p and q_{CSM}). Firstly, small differences are observed for the different types of analyses for yield strain ε_y.

Secondly, the formation of plastic hinges clearly controls the resistance of the beam, leading to a plastic load of 291 N/mm, much lower

Table 9
Detailed results at specific load levels.

Load level	q_{el}^{SD}	q_{el}^{LD}	$q_{el\text{-}pl}^{LD}$	w_{el}^{SD}	w_{el}^{LD}	$w_{el\text{-}pl}^{LD}$	ε_t	ε_b
q_y	103.1	104.3	102.4	1.9	1.8	1.8	0.131%	−0.116%
q_p	154.7	2769.7	203.8	2.8	13.0	4.7	1.551%	−0.676%
q_{CSM}	155.0	4012.3	211.8	2.8	15.1	5.1	1.964%	−0.806%

than the equivalent large displacement load that corresponds to the same level of strain. Finally, membrane strains strongly affect the plastic resistance, that is 1.65 times larger than the corresponding elastic resistance, in excess of the shape factor for rectangular cross-sections. Hence, the direct calculation of the yield/plastic load q using eq. (44) directly from the moment-curvature relationship for cross-section C is too conservative.

It can be concluded that even for beams that behave according to Case 2, the plastic resistance and the design resistance is strongly affected by axial forces that develop due to the axial restraint at the supports.

5.2. Slender beam strip

Consider a simply supported beam strip (see Fig. 6) with length $2a = 900$ mm, thickness $t = 8$ mm, width $b = 100$ mm, loaded with a uniformly distributed load q_0 over a central segment of length $2c = 270$ mm and with $I_2 = 64I$ and $A_2 = 4A$, where I is the moment of inertia and A is the area of the side segments. Fig. 17 depicts the linear elastic solution, large displacement elastic solution and large displacement elastic-plastic solution, all calculated numerically using ABAQUS and applying the analytical equations derived in section 3. Firstly, the first order solution (linear elastic) is almost perfectly superimposed with the large displacement elastic solution, showing that membrane effects are not relevant for this example (Case 3). Secondly, the numerical elastic-plastic curve is well approximated by the analytical solution.

Fig. 18 compares the deformed shape for two load levels: load q_p corresponding to the plastic resistance of cross-section C and load q_{CSM} corresponding to the strain ε_{CSM} at the same cross-section.

Fig. 19 illustrates the variation of the total top and bottom strain at point C, showing that there is a marked plastic plateau with no noticeable membrane contribution.

The deformation criterion (27 mm) given by eq. (34b) leads to a maximum resistance of 143.4 N/mm. Table 8 summarizes relevant results for practical application for three load levels (q_y, q_p and q_{CSM}). Firstly, the small displacement results present large differences (> 100%) when compared to large displacement results because of the slenderness of this beam strip.

Secondly, membrane strains increase the plastic resistance by 2.99 times the corresponding elastic resistance. Finally, application of the CSM resistance criterion leads to a resistance of 42.6 N/mm, well below the resistance of 143.4 N/mm that is proposed by the 3% deformation criterion.

It can be concluded that for beams that behave according to Case 3, membrane resistance controls the behaviour of the beam and the usual deformation criterion of 3% is not applicable, leading to very large errors.

5.3. Beam strip with intermediate slenderness

Consider a simply supported beam strip (see Fig. 6) with length $2a = 400$ mm, thickness $t = 12$ mm, width $b = 100$ mm, loaded with a uniformly distributed load q_0 over a central segment of length $2c = 80$ mm and with $I_2 = 64I$ and $A_2 = 4A$, where I is the moment of inertia and A is the area of the side segments. Fig. 20 depicts the linear elastic solution, large displacement elastic solution and large displacement elastic-plastic solution, all calculated numerically using ABAQUS and applying the analytical equations derived in section 3. Firstly, the first order solution (linear elastic) is almost perfectly superimposed with the large displacement elastic solution, showing that membrane effects are not relevant for this example (Case 3). Secondly, the numerical elastic-plastic curve is well approximated by the analytical solution.

Fig. 21 compares the deformed shape for two load levels: load q_p corresponding to the plastic resistance of cross-section C and load q_{CSM} corresponding to the strain ε_{CSM} at the same cross-section.

Fig. 22 illustrates the variation of the total top and bottom strain at point C, showing that there is a marked plastic plateau with no noticeable membrane contribution.

The deformation criterion (12 mm) given by eq. (34b) leads to a maximum resistance of 399.3 N/mm. Table 9 summarizes relevant results for practical application for three load levels (q_y, q_p and q_{CSM}). The results present the features of both previous cases, requiring the consideration of membrane forces and strongly deviating from small displacement theory.

The 3% deformation criterion overestimates the resistance of the beam (399.3 N/mm *vs* 211.8 N/mm).

As for case 3, It can be concluded that for beams that behave according to Case 1, the consideration of large displacements is required for meaningful results.

6. Conclusions

This paper presented a mechanically consistent model for the nonlinear behaviour of the face plate component which is typical whenever a steel member is connected to the web of an open I-section or to the face of a rectangular hollow section. A practical design methodology is proposed that is based on closed form analytical expressions.

The following conclusions could be reached:

- The model can capture very accurately, the plate-like behaviour of the face plate component in the elastic large displacement range, which is indispensable in this case as membrane stresses are mobilized early and in the design zone of the force displacement curve.
- The proposed methodology to estimate analytically, the elastic plastic large displacement behaviour of the faceplate component gives good results when compared to advanced numerical simulations.
- The application of the Continuous Strength Method strain limits provides an appropriate criterion for the establishment of the design resistance, solving the shortcomings of empirical criteria, such as the 3% deformation limit, or the use of resistances directly based on yield-line theory.
- Membrane forces significantly affect the resistance, even for stocky beam strips.

The proposed methodology is easy to use as it relies on closed-form analytical equations that yield the exact solution to the large displacement elastic response of the equivalent beam strip.

The proposed model relies on the calculation of an equivalent width. This equivalence was established for the initial linear elastic response. An equivalent width needs to be calibrated for plastic conditions. This will be addressed in the near future by the authors.

CRediT authorship contribution statement

Luís Simões da Silva: Writing – review & editing, Writing – original draft, Validation, Methodology, Investigation, Formal analysis, Conceptualization. **Trayana Tankova:** Writing – review & editing, Writing – original draft, Validation, Methodology, Investigation, Formal analysis, Conceptualization.

Declaration of competing interest

I declare on behalf of myself and all the authors that there is no conflict of interest.

Data availability

Data will be made available on request.

Acknowledgments

This work was partly financed by:

- FCT / MCTES through national funds (PIDDAC) under the R&D Unit Institute for Sustainability and Innovation in Structural Engineering (ISISE), under reference UIDB / 04029/2020, and under the Associate Laboratory Advanced Production and Intelligent Systems (ARISE) under reference LA/P/0112/2020.

References

[1] J. Conde, L. Simões da Silva, A.F. Santos, M. Lemma, T. Tankova, A model for the initial stiffness of the face plate component, Eng. Struct. 295 (116836) (2023) 2023.
[2] EN 1993-1-8, Eurocode 3: Design of Steel Structures – Part 1–8: Design of Joints, European Committee for Standardization, Brussels, Belgium, 2005.
[3] L.F.C. Neves, F.C.T. Gomes, Semi-rigid behavior of beam-to-column minor-axis joints, in: Proceedings of the IABSE International Colloquium on Semi Rigid Structural Connections, Istanbul, Turkey, 1996, pp. 207–216.
[4] L.A.P. Silva, L.F.C. Neves, Gomes FCT, Rotational stiffness of rectangular hollow sections composite joints, J. Struct. Eng. 129 (2003) (2003) 487–494, https://doi.org/10.1061/(asce)0733-9445(2003)129:4(487).
[5] A.Y. Park, Y.C. Wang, Development of component stiffness equations for bolted connections to RHS columns, J. Constr. Steel Res. 70 (2012) 137–152.
[6] A. Ghobarah, S. Mourad, R.M. Korol, Moment-rotation relationship of blind bolted connections for HSS columns, J. Constr. Steel Res. 40 (1) (1996) 63–91.
[7] M. Mahmood, W. Tizani, A component model for column face in bending of extended HolloBolt connections, J. Constr. Steel Res. 182 (2021) 106655, https://doi.org/10.1016/j.jcsr.2021.106655.
[8] Y. Dongchen, K. Ke, Y. Chen, Stiffness model for "column face in bending" component in tensile zone of bolted joints to SHS/RHS column, Steel Compos. Struct. 38 (6) (2021) 637–656 (2021).
[9] Y. Harada, L. Simões da Silva, Three-dimensional macro-modelling of rectangular steel hollow section beam-to-column joints under cyclic loading – part 1: cyclic out-of-plane behaviour of single isolated column plate, J. Constr. Steel Res. 162 (2019) 105713.
[10] Y. Harada, L. Simões da Silva, Three-dimensional macro-modelling of rectangular steel hollow section beam-to-column joints under cyclic loading – part 2: modelling by an extended component-based approach, J. Constr. Steel Res. 162 (2019) 105714.
[11] N. Kosteski, J.A. Packer, Longitudinal plate and through plate-to-hollow structural section welded connections, *J. Struct. Eng.* ASCE 129 (4) (2003) 478–486.
[12] L. Gardner, X. Yun, F. Walport, The continuous strength method – review and outlook, Eng. Struct. 275 (2023) 114924.
[13] prEN 1993-1-14, Eurocode 3: Design of Steel Structures – Part 1–14: Design by FEM, European Committee for Standardization, Brussels, Belgium, 2023.
[14] L. Neves, L. Simões da Silva, P. Vellasco, A model for predicting the stiffness of beam to concrete filled column and minor axis joints under static monotonic loading, in: B. Hoffmeister, O. Hechler (Eds.), Eurosteel 2005 – 4th European Conference on Steel and Composite Structures – Research – Eurocodes – Practice C, Druck und Verlagshaus Mainz GmbH, Aachen, 2005, pp. 4.10.131-138.
[15] M.S. Lemma, C. Rebelo, J. Conde, L. Simões da Silva, Experimental and numerical characterization of column webs/faces loaded out-of-plane in steel joints, 2024.
[16] J.P. Jaspart, K. Weynand, Design of Joints in Steel and Composite Structures, ECCS and Ernst & Sohn, Wiley, Brussels, Belgium, 2016.
[17] L. Simões da Silva, H.D. Craveiro, R.A. Simões, T. Tankova, R.J.T. Costa, INNO3DJOINTS - Innovative 3D Joints for Robust and Economic Hybrid Tubular Construction - Final Report, Brussels, Belgium, 2021.
[18] J. Wardenier, G.J. Van Der Vegte, D.K. Liu, Chord stress function for rectangular hollow section X and T joints, in: Proceedings of the Seventeenth International Offshore and Polar Engineering (ISOPE) Conference, Lisbon, Portugal, 2007.
[19] F.C.T. Gomes, J.P. Jaspart, R. Maquoi, Moment capacity of beam-to-column minor-axis joints, in: Proceedings of the IABSE International Colloquium on Semi-Rigid Structural Connections, Istanbul, Turkey, IABSE, 1996, pp. 319–326.
[20] N. Yeomans, Rectangular hollow section column connections using the Lindapter HolloBolt, Tubul. Struct. VIII (1998) 559–566.
[21] BCSA, SCI, Joints in steel construction : Simple Joints to Eurocode 3, 2011.
[22] Z.Y. Wang, Q.Y. Wang, Yield and ultimate strengths determination of a blind bolted endplate connection to square hollow section column, Eng. Struct. 111 (Mar. 2016) 345–369.
[23] X.-L. Zhao, Deformation limit and ultimate strength of welded T-joints in cold-formed RHS sections, J. Constr. Steel Res. 53 (2) (Feb. 2000) 149–165.
[24] X. Yun, L. Gardner, Stress strain curves for hot-rolled steels, J. Constr. Steel Res. 133 (2017) 36–46.
[25] K. Washizu, Variational Methods in Elasticity and Plasticity, 3rd edition, Pergamon Press, 1982.
[26] Mathworks, MATLAB® Primer, 2023 [online]. Last accessed 14.2.2024. Available at: https://www.mathworks.com/products/matlab.html.
[27] Simulia, Abaqus User Manual, Dassault systems Simulia Corp, 2021 [online]. Last accessed 06/01/2023. Available at: https://help.3ds.com/HelpProductsDS.aspx.
[28] L. Simões da Silva, A. Girão Coelho, E.L. Neto, Equivalent post-buckling models for the flexural behavior of steel connections, Comput. Struct. 77 (2000) 615–624, https://doi.org/10.1016/S0045-7949(00)00015-8.
[29] W.F. Chen, T. Atsuta, Theory of beam-columns, in: In-Plane Behavior and Design Vol 1, McGraw-Hill, 1976.
[30] C. Faella, V. Piluso, G. Rizzano, Structural Steel Semirigid Connections – Theory, Design and Software, CRC Press, 2000.